Sensors and Materials, Vol. 31, No. 2 (2019) 645–659
MYU Tokyo

S & M 1803

Fabrication of Inverse Opal Photonic Crystals with Mesopores Using Binary Colloidal Co-assembly Method for Signal Enhancement in Formaldehyde Detection

Yuto Komori,[1] Hiroaki Murakami,[1] Taiki Kimura,[1] and Takeshi Onodera[2*]

[1]Graduate School of Information Science and Electrical Engineering, Kyushu University,
744 Motooka, Nishi-ku, Fukuoka 819-0395, Japan
[2]Faculty of Information Science and Electrical Engineering, Kyushu University,
744 Motooka, Nishi-ku, Fukuoka 819-0395, Japan

(Received October 25, 2018; accepted January 21, 2019)

Keywords: inverse opal, photonic crystal, binary colloidal crystal, mesopore, formaldehyde, Fluoral-P

In this study, inverse opal photonic crystals (IOPCs) with mesopores (diameter, 2–50 nm) were fabricated by the optimization of the size ratio of large to small polystyrene (PS) nanoparticles used as the template of the IOPCs and the concentration of the precursor forming the structure of the IOPCs. The generation of cracks and defects on the obtained IOPCs was avoided by using the co-assembly method, which is a self-organized fabrication method for IOPCs using nanoparticles of a polymer such as PS as a template in a precursor solution. 4-Amino-3-pentan-2-one (Fluoral-P) was infiltrated into the IOPCs, and the edge of the photonic band gap of an IOPC fabricated using 350 and 50 nm PS nanoparticles (50 nm-350IOPC) was matched with part of the fluorescence wavelength range of 3,5-diacetyl-1,4-dihydro-2,6-lutidine (DDL), which is a substance emitting fluorescence resulting from the reaction of Fluoral-P with formaldehyde. It was found that introducing mesopores into 350IOPC with infiltrated Fluoral-P was effective for enhancing the signal in formaldehyde detection.

1. Introduction

Recently, photonic crystal (PC)-based sensors for the detection of chemical substances have been proposed.[1–3] PCs are structures having a periodic distribution of the refractive index, and a photonic bandgap, in which a certain wavelength range of light cannot exist, appears in the structure. In particular, in the case of a PC with a 100-nm-order pitch, UV-visible wavelengths in the light irradiated from outside the PC cannot enter the crystal and are strongly reflected, resulting in the crystal having a structural color. The structural color depends on the physical properties of the structure such as its refractive index and the distance between crystal planes.[4] Therefore, the structural color will change when substances that affect the refractive index or the distance between crystal planes enter the structure. PC-based sensors that utilize this change in structural color can be developed.

*Corresponding author: e-mail: onodera@ed.kyushu-u.ac.jp
https://doi.org/10.18494/SAM.2019.2168

ISSN 0914-4935
https://myukk.org/

Among the PCs, those that are formed by the self-organization of same-size nanoparticles in a colloid solution during the evaporation of the solvent are called colloidal PCs. This fabrication method has attracted a lot of attention because it is easy to obtain three-dimensional PCs at a low cost. A fabrication method for inverse opal photonic crystals (IOPCs), i.e., the co-assembly method, proposed by Hatton *et al.* makes it easy to fabricate IOPCs with high porosity, which have been used for gas sensing.[5] Because PCs do not have specific reactivity to chemical substances, to realize specificity, they must be formed with a functional material that reacts with a target substance. Alternatively, the surface of an IOPC modified with a reagent can interact with the target substance.

For example, a 4-amino-3-pentan-2-one (Fluoral-P)-infiltrated IOPC has been proposed for the detection of formaldehyde, and IOPCs filled with an aggregation-induced emission (AIE) substance have been proposed for volatile organic compound (VOC) detection.[6,7] To detect formaldehyde specifically, an IOPC formed with SnO_2 was proposed.[8] Increasing the surface area of an IOPC is one of the ways of signal enhancement, which can be achieved by introducing small pores into the IOPC. Wang *et al.* obtained a binary IOPC from a multilayered trimodal colloidal crystal using large PS, medium-size polymethyl methacrylate (PMMA), and small SiO_2 particles, which were used as the basic material of the IOPC's structure.[9]

In this study, we chose formaldehyde as the target substance and proposed a fabrication method for an IOPC with mesopores using a binary colloidal co-assembly method for signal enhancement in formaldehyde detection. To increase the loading capacity of Fluoral-P, we introduced mesopores (diameter, 2–50 nm) into IOPCs. We formed IOPCs with mesopores on a glass slide using the co-assembly method with tetraethyl orthosilicate (TEOS) solution containing 350 and 50 nm polystyrene (PS) nanoparticles. We evaluated the detection capability of IOPCs with mesopores for acetone and the effect of infiltrating a mesoporous IOPC with Fluoral-P on signal enhancement.

2. Experimental Methods

2.1 Materials and instruments

TEOS and Fluoral-P were purchased from Tokyo Chemical Industry. Methanol and ethanol for pesticide residue and PCB analysis were purchased from FUJIFILM Wako Pure Chemical. Formaldehyde solution was obtained from Nacalai Tesque. 2.5% PS 0.5 mm, 2.5% PS 0.1 mm, 2.5% PS 0.35 mm, and 2.6% PS 0.05 mm microspheres were obtained from Polysciences. All other chemicals were purchased from either FUJIFILM Wako Pure Chemical or Kanto Chemical. Milli-Q deionized water was obtained from a Milli-Q-system (Merck Millipore). Glass slides (S2441; 76 × 26 mm^2) manufactured by Matsunami Glass Industry were used as base plates of IOPCs. Scanning electron microscopy (SEM) systems, S-3400N type II and SU8000 (Hitachi High-Technologies), were used for the observation of IOPC films. A fiber spectrometer, FLAME-S-XR1-ES with a 5 mm slit (Ocean Optics) and a tungsten halogen light source (HL-2000, Ocean Optics), a reflection probe (R400-7-UV/VIS, Ocean Optics), and a reflection probe holder (RPH-1, Ocean Optics) were used to measure the reflection spectra of IOPCs.

2.2 Principle

When reflection occurs at the first and second layers of a PC and the optical path difference between the light reflected at the first and second layers is equal to the wavelength of the irradiated light or to an integer multiple of the wavelength, interference will occur and strong light will be observed. For the distance between the planes in the crystal lattice (d), glancing angle (θ), the wavelength of incident light (λ), and the average refractive index of the crystal (n), the optical path difference is $2nd\sin\theta$. Thus, if

$$m\lambda = 2nd\sin\theta, \ (m \text{ is an integer}) \tag{1}$$

is satisfied, the intensity of the reflected light will increase. This equation is called Bragg's formula. The refractive index of the particle (n_p), the refractive index of the medium (n_m), the volume ratio of particles (ψ), and n are related by the following equation:[1,2,10]

$$n = \sqrt{n_p^2\psi + n_m^2(1-\psi)}\,. \tag{2}$$

The inverse opal structure is a face-centered-cubic (fcc) lattice structure, the same as the opal structure. When white light is irradiated onto the (111) plane of a colloid PC film having an fcc lattice structure, light is strongly reflected at a wavelength called the stopband wavelength λ, which is represented by the following equation:[1,2,10,11]

$$\lambda = 2\sqrt{\frac{2}{3}}D\sqrt{n^2 - \sin^2\theta}\,. \tag{3}$$

Here, D is the interparticle distance (= diameter of particles, or diameter of pores in the case of an inverse opal) and θ is the incident angle of light.

2.3 Fabrication of 350IOPC by co-assembly method

An IOPC without mesopores was fabricated by the co-assembly method.[5] The IOPC silica (SiO_2) structure was obtained by the sol-gel reaction of TEOS, hydrochloric acid, ethanol, and H_2O. PS particles of 350 nm diameter were used as a template for the fabrication of the IOPC. Firstly, a precursor solution of the IOPC matrix was prepared by mixing 2.0 g of TEOS, 2.0 g of 0.1 mol/L hydrochloric acid, and 3.0 g of ethanol, then stirring at room temperature for 1 h. Next, 0.10 mL of the precursor solution and 1.0 mL of 0.35 mm microspheres were added to 20 mL of Milli-Q water, then the mixture was stirred. After that, a glass slide was held vertically in a Teflon cup loaded with the mixture solution. Before use, the glass slide was cleaned by heating at 90 °C in Standard Clean 1 (SC1) solution (with ammonia solution, hydrogen peroxide, and Milli-Q water at 1:1:5 ratio). Then, a PC film was formed on the glass slide by evaporating the solvent by heating the cup at 65 °C on a hotplate for 30 h. Finally, to obtain an IOPC film with

the PS particles in the PC film removed selectively, the PC film on the glass slide was heated in a programmable electric heater at 500 °C for 2 h (lamp time: 4 h). The surface of the obtained IOPC film was observed by SEM.

2.4 Fabrication of IOPC with mesopores (50 nm-350IOPC and 100 nm-350IOPC) by binary colloidal co-assembly method

Figure 1 shows the fabrication process for an IOPC with mesopores by the binary colloidal co-assembly method. A precursor solution was prepared in the same manner as in the case of 350IOPC, then 0.10 mL of the precursor solution and 1.0 mL of 0.35 mm microspheres were placed in 20 mL of Milli-Q water, then the mixture was stirred. Next, x mL (or y mL) of 50 nm (or 100 nm) PS nanoparticle solution was added to the mixture, then the mixture was stirred. The subsequent process was the same as in the case of 350IOPC. When many defects or cracks were observed by SEM upon increasing the amount of PS solution in IOPC, we concluded that the amount of precursor solution was insufficient. In such cases, we increased the amount of the precursor solution that was added to the solution by 0.10 mL.

2.5 Nonspecific detection of acetone using IOPCs with mesopores

The nonspecific detection of acetone gas was performed to demonstrate that the peak in the reflection spectrum of an IOPC is markedly shifted by the large change in refractive index associated with capillary condensation in the IOPC when a gas enters the IOPC. We determined whether 350IOPC, 50 nm-350IOPC, or 100 nm-350IOPC was the most sensitive IOPC for detecting acetone.

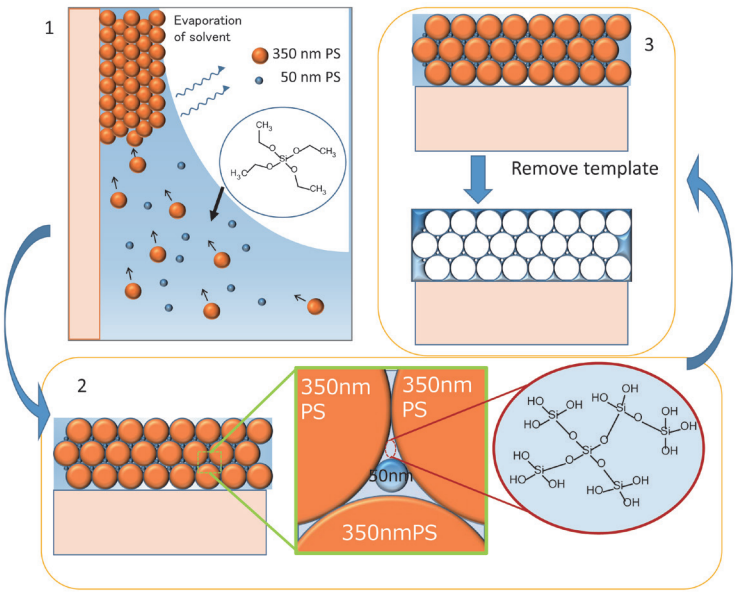

Fig. 1. (Color online) Fabrication process for IOPC with mesopores by binary colloidal co-assembly method.

The most sensitive IOPC should have the largest number of mesopores; thus, acetone detection was carried out to find which of the three IOPCs had the largest number of mesopores. The concentration of acetone at which it can undergo capillary condensation in 20 nm pores was determined by the Kelvin equation.[12] 6.944×10^{-3} mol of acetone was calculated from the ideal gas law, which was placed in a 750 mL screw vial and completely evaporated.

Figure 2 shows the experimental setup. Spectral measurement was carried out with the glancing angle θ set at 90°. The reflection probe holder was put on the three IOPCs at each measurement using a guide for fixing the measurement position. The reflection spectra of 350IOPC, 50 nm-350IOPC, and 100 nm-350IOPC were measured before exposure to acetone. Each IOPC was placed in the 750 mL vial and exposed to gaseous acetone for 10 min, then the relative peak shift was determined by measuring the reflection spectra. The relative peak shift $D\lambda$ was calculated using the following equation:

$$\Delta\lambda = (\lambda - \lambda_0) / \lambda_0 \times 100 \,. \tag{4}$$

Here, λ and λ_0 are the peak wavelengths in the reflection spectra of the IOPC before and after exposure to acetone, respectively. After measurement, the IOPCs were left in room air for 20 min to allow the evaporation of the acetone inside the crystals, and it was confirmed that the reflection peak of each IOPC had returned to its original position. This experiment was performed three times.

2.6 Specific detection of formaldehyde using IOPCs with mesopores

We investigated whether introducing mesopores into an IOPC was effective in proving its performance in formaldehyde detection. 1.0 mL of 2.5% PS 0.5 mm microspheres was used for the fabrication of a 500 nm IOPC (500IOPC) in the same manner as in the case of 350IOPC. 100 μL of 1.0 wt% Fluoral-P in methanol solution was added dropwise to 50 nm-350IOPC,

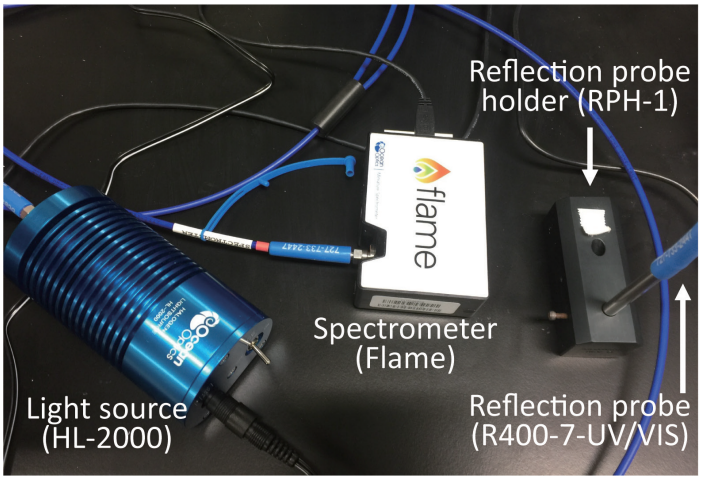

Fig. 2. (Color online) Experimental setup for spectral measurement on IOPCs.

350IOPC, 500IOPC, or a cleaned glass slide, then the solvent was allowed to evaporate. The reflection spectrum on each IOPC was measured as well as that on the glass slide for reference. After that, each IOPC and the glass slide were placed in the 750 mL vial filled with saturated formaldehyde gas for 10 min and the reflection spectral change was measured for each IOPC and the glass slide. This measurement was performed three times.

3. Results and Discussion

3.1 Fabrication of 350IOPC by co-assembly method

An IOPC that generated brilliant structural colors was obtained using the co-assembly method with 350-nm-diameter PS nanoparticles. The exterior of the obtained 350IOPC is shown in Fig. 3. The IOPC generated green and yellow structural colors. Figure 4 shows the reflection spectrum of the IOPC, in which a sharp peak at 517 nm was observed.

Figure 5 shows a SEM image of the surface of 350 IOPC. The image of the fabricated IOPC indicates that the (111) plane of an fcc lattice structure formed and that a high-quality IOPC film was obtained using 350 nm PS particles.

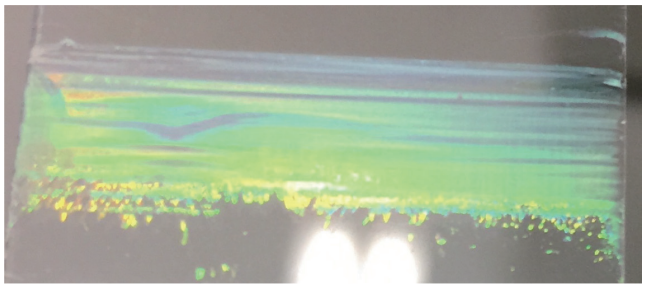

Fig. 3. (Color online) IOPC fabricated with 350 nm PS nanoparticles on a glass slide.

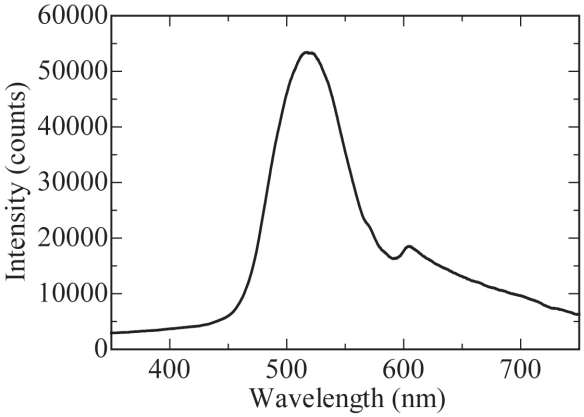

Fig. 4. Reflection spectrum of IOPC fabricated with 350 nm PS nanoparticles.

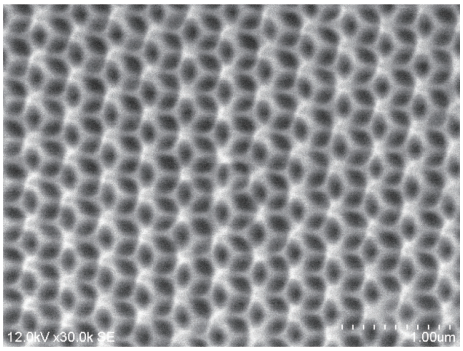

Fig. 5. SEM image of IOPC fabricated with 350 nm PS nanoparticles.

3.2 Fabrication of 50 nm-350IOPC by binary colloidal co-assembly method

First, the volume of the 50 nm (or 100 nm) PS nanoparticle solution (x) was set with reference to previous studies on the fabrication of binary colloidal crystals (bCCs) with fabricated periodic structures using a colloid solution with dispersed colloid particles.[13–15] In the study of bCCs, it has been investigated whether a periodic structure of large particles L with small particles S placed between the large particles can be formed. It has been reported that two parameters, the diameter ratio $\gamma_{S/L}$ (diameter of S to diameter of L) and particle number ratio $N_{S/L}$ (the number of S to the number of L in a solution), are important factors that determine the formability of a structure. In previous studies, $N_{S/L}$ values of less than 3.6 and between 3.9 and 4.1 resulted in the formation of a high-quality structure.[13,14] However, in these studies, only two sizes of particles were used to form the crystal structure by self-assembly without a precursor solution. These parameters cannot be determined independently because when one parameter changes, the other one also changes; however, $N_{S/L} = 3.6$ was chosen as a guide value in this study.

Table 1 shows the numbers of particles in 1 mL of the PS nanocolloidal solutions used in this study. The amount of the additional PS nanoparticle solution required to adjust $N_{S/L}$ to 3.6 was calculated to be $x = 0.01048$. Next, the effect of adding this amount of the PS nanoparticle solution was investigated. Figure 6 shows a SEM (SU8000) image of the obtained 50 nm-350IOPC (50 nm PS, $x = 0.01048$). The figure shows that an fcc lattice structure was formed with satisfactory stability that had mesopores with a diameter of less than 50 nm scattered in the silica structure. Thus, the co-assembly method using template particles of two sizes can be realized for appropriate particle number ratios and diameter ratios. However, the positioning of the mesopores was irregular, with no mesopores existing in some parts of the IOPC. The reason for this irregularity was given in previous studies; it is difficult to fix the positions of

Table 1
Numbers of particles in 1 mL of PS nanocolloidal solutions.

Diameter (nm)	Number of particles (/mL)
50	3.64×10^{14}
100	4.55×10^{13}
350	1.06×10^{12}

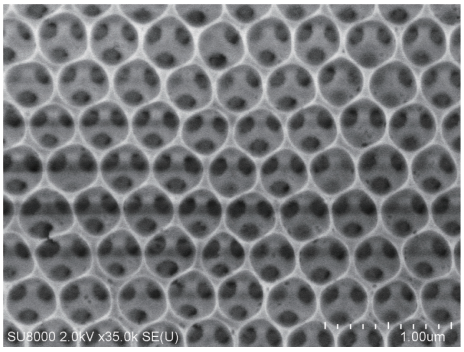

Fig. 6. SEM (SU8000) image (high magnification) of the obtained 50 nm-350IOPC (50 nm PS, $x = 0.01048$). Scale bar = 1 μm.

small particles because they can move freely through the spaces between the large particles when the diameter ratio is $\gamma_{S/L}$ 0.1547.[13,14] It is also possible that the difficulty in observing the mesopores was due to shrinkage to a size beyond the visibility range of the SEM when the IOPC was heated at 500 ℃ to remove template PS nanoparticles. Figures 7 and 8 show that the fcc lattice structure was also satisfactorily maintained over a large area. Therefore, it appears that x can be further increased.

Figure 9 shows a SEM (SU8000) image of an obtained 50 nm-350IOPC with x = 0.165 and 0.2 mL of the precursor solution. Some cracks and defects were observed in a large area, and the fcc lattice structure was also observed. Furthermore, mesopores with a diameter of about 50 nm regularly positioned in the silica structure of the IOPC were observed clearly. The corresponding reflection spectrum is shown in Fig. 10. The peak of the reflection spectrum in Fig. 10 was sharp, similarly to that of the spectrum of 350IOPC without mesopores in Fig. 4. Thus, 50 nm-350IOPC can be applied to sensing. The peak wavelength in Fig. 10 was at 502 nm lower than that in Fig. 4. The porosity of the IOPC increased owing to the many mesopores introduced into the IOPC; thus, the average refractive index of the IOPC given by Eq. (2) slightly decreased, namely, the right side of Eq. (3) decreased.

Fig. 7. SEM (SU8000) image of an obtained 50 nm-350IOPC (50 nm PS, x = 0.01048). Scale bar = 5 μm.

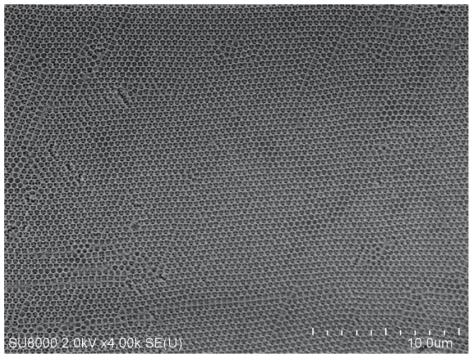

Fig. 8. SEM (SU8000) image of an obtained 50 nm-350IOPC (50 nm PS, x = 0.01048). Scale bar = 10 μm.

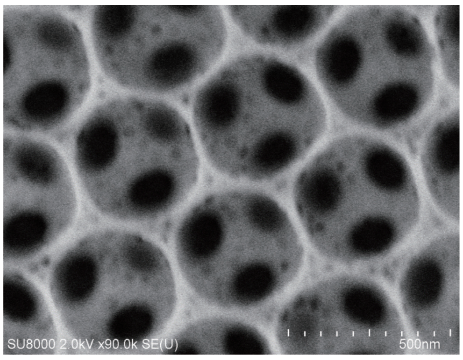

Fig. 9. SEM (SU8000) image (high magnification) of an obtained 50 nm-350IOPC (50 nm PS, x = 0.165, 0.2 mL precursor solution). Scale bar = 500 nm.

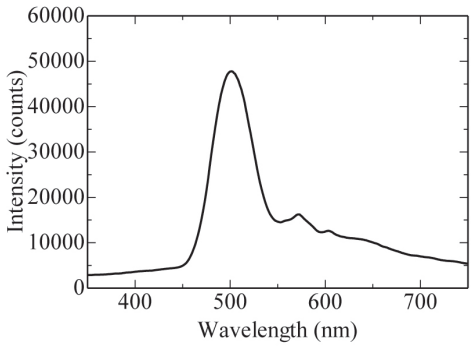

Fig. 10. Reflection spectrum of 50 nm-350IOPC (50 nm PS, x = 0.165, 0.2 mL precursor solution).

For this IOPC, the diameter ratio $\gamma_{S/L}$ and the particle number ratio $N_{S/L}$ were 0.1429 and 56.66, respectively. These values were considerably different from the guide values, because the precursor solution used in this study had non-negligible viscosity. We concluded that 0.20 mL of precursor solution and $x = 0.165$ were suitable conditions in this study for fabricating 50 nm-350IOPC. SEM images of the IOPCs obtained under the other conditions are shown in Table S1 (found online).

3.3 Fabrication of 100 nm-350IOPC using binary colloidal co-assembly method

100 nm-350IOPC was fabricated in the same manner as in the case of 50 nm-350IOPC. Figures 11 and 12 show SEM (SU8000) images of the obtained 100 nm-350IOPC (100 nm PS, $y = 0.045$). Although some defects can be observed in Fig. 11, most of the IOPCs maintained the fcc lattice structure. Note that $y = 0.045$ is almost the maximum amount of the PS nanoparticle solution that can be added. Figure 12 shows that many pores can be made with 100 nm PS nanoparticles scattered in the silica structure as templates. The peak of the corresponding reflection spectrum in Fig. 13 was sharp, similarly to that of the spectrum of 350IOPC without mesopores in Fig. 4. Thus, 100 nm-350IOPC can also be applied to sensing.

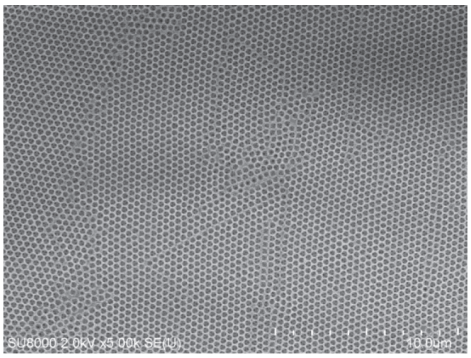

Fig. 11. SEM (SU8000) image of the obtained 100 nm-350IOPC (100 nm PS, $y = 0.045$, 0.2 mL precursor solution). Scale bar = 10 μm.

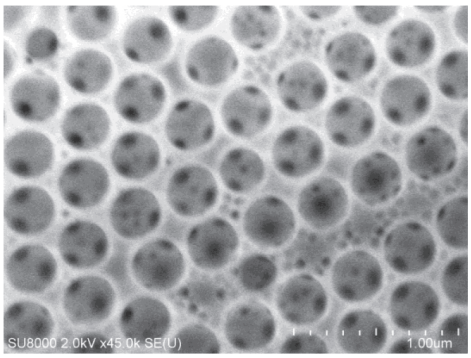

Fig. 12. SEM (SU8000) image (high magnification) of the obtained 100 nm-350IOPC (100 nm PS, $y = 0.045$, 0.2 mL precursor solution). Scale bar = 1 μm.

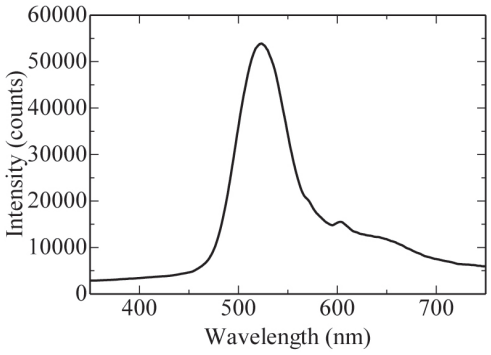

Fig. 13. Reflection spectrum of 100 nm-350IOPC (100 nm PS, $y = 0.045$, 0.2 mL precursor solution).

The peak wavelength in Fig. 13 was at 523 nm, lower than that in Fig. 4. The porosity of the IOPC increased owing to the many pores with a diameter of less than 100 nm introduced into the IOPC; thus, the average refractive index of the IOPC given by Eq. (2) slightly decreased. However, the size of the introduced pores was larger than that of the mesopores obtained using 50 nm PS. This increased the value of D in Eq. (3), shifting the peaks to a higher wavelength.

For this IOPC, the diameter ratio $\gamma_{S/L}$ and the particle number ratio $N_{S/L}$ were 0.2857 and 1.932, respectively. These values were considerably different from the guide values in this study, because when the diameter ratio $\gamma_{S/L}$ is larger than 0.2247, it is difficult for small particles to position themselves in a line between large particles and possible spaces where small particles can be positioned are limited. It is necessary to estimate the number of small particles to a lesser extent. SEM images obtained under the other conditions are shown in Table S2 (found online).

3.4 Nonspecific detection of acetone using IOPCs with mesopores

Figure 14 shows the relative peak shifts when 350IOPC, 50 nm-350IOPC, and 100 nm-350IOPC were exposed to acetone. When 50 nm-350IOPC was used, its relative peak shift was the largest among the three IOPCs. From Eq. (3), the reflectance peak wavelength λ was found to depend on the interparticle distance D and the average refractive index of the crystal (n) at a fixed incident angle of light. Each IOPC was made of SiO_2; therefore, D for each IOPC did not vary its exposure to acetone, meaning that the peak shift was probably due to the change in n following the infiltration of acetone into the IOPCs. According to a previous study on gas sensing using porous SiO_2, the changes in its optical characteristics are due to the capillary condensation and physical adsorption of gaseous molecules by the van der Waals force.[3] It was not confirmed whether there were nanosize cracks allowing capillary condensation on 350IOPC; however, it is likely that 350IOPC did not have a significant number of mesopores. Thus, the reflection peak shift indicated that acetone was adsorbed on the surface of 350IOPC by physical adsorption.

Figure 12 indicates that pores with a diameter of less than 100 nm were introduced into the SiO_2 structure of 100 nm-350IOPC; however, the relative peak shift after acetone exposure was

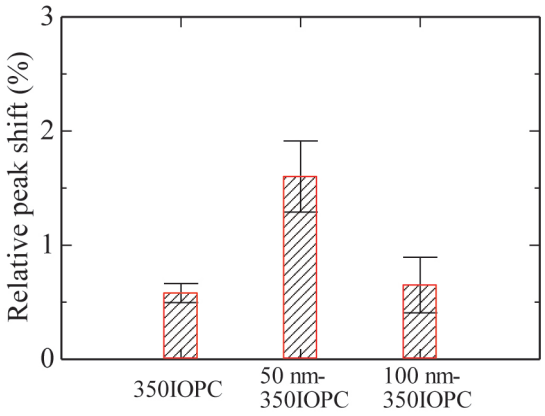

Fig. 14. (Color online) Relative peak shift of each IOPC after acetone exposure.

similar to that of 350IOPC. Thus, hardly any capillary condensation of acetone is considered to have occurred, and acetone molecules were mainly adsorbed on 100 nm-IOPC by physical adsorption. From these results, when the porosity and surface area increased, the relative peak shift was hardly affected; thus, simply increasing the surface area per unit area did not affect the relative peak shift.

When 50 nm-350IOPC was used, its relative peak shift was about two times higher than those of the other IOPCs. The porosity and surface area were greater than those of 350IOPC. However, simply increasing the surface area per unit area is not expected to affect the peak shift; therefore, it is probable that the efficient capillary condensation of acetone occurred. These results show that 50 nm-350IOPC has more mesopores with a diameter less than 50 nm, causing the capillary condensation of acetone, than the other IOPCs, and that improved vapor detection and sensitivity can be achieved by introducing numerous mesopores into IOPCs.

3.5 Specific detection of formaldehyde using IOPCs with mesopores

Figure 15 shows the reaction process of Fluoral-P and formaldehyde. Fluoral-P reacts with formaldehyde to form the fluorescent compound 3,5-diacetyl-1,4-dihydro-2,6-lutidine (DDL).[6,16] This reaction proceeds readily in a short time, and Fluoral-P does not react with other compounds such as aldehydes to form fluorescent compounds. Zhan *et al.* reported that a Fluoral-P-infiltrated IOPC has selectivity to formaldehyde among eight kinds of gases, such as acetaldehyde, propaldehyde, and methanol.[6] Therefore, the high-sensitivity detection and quantification of formaldehyde with selectivity are possible using Fluoral-P.

Figure 16 shows the reflection spectral change observed on 50 nm-350IOPC before and after formaldehyde exposure. The dashed black line represents the normalized reflectance

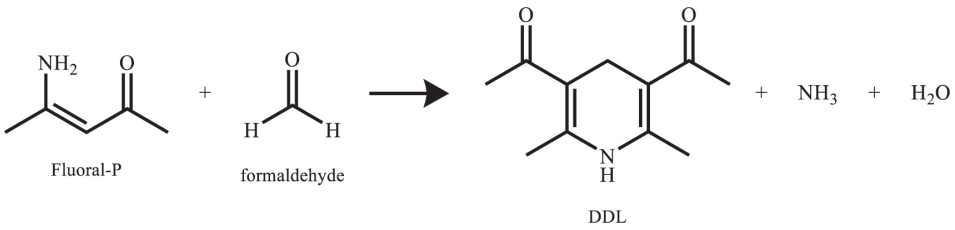

Fig. 15. Reaction process of Fluoral-P and formaldehyde.

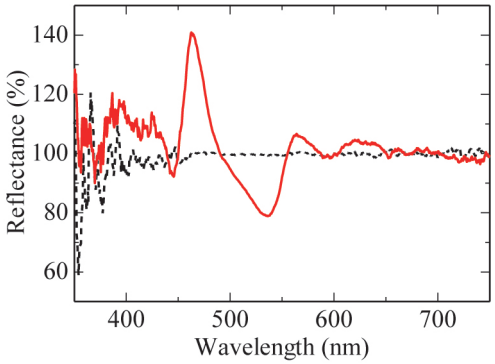

Fig. 16. (Color online) Reflection spectral change on 50 nm-350IOPC before (dashed black line) and after (red line) formaldehyde exposure.

spectrum of 50 nm-350IOPC with infiltrated Fluoral-P before formaldehyde exposure. Ideally, the reflectance should be 100% at all wavelengths; however, a fluctuation caused by noise from instruments was observed below 450 nm and above 750 nm. The solid red line represents the normalized reflectance spectrum of 50 nm-350IOPC with infiltrated Fluoral-P after formaldehyde exposure for 10 min. Compared with the reflectance before exposure, the reflectance after exposure increased at around 463 nm. Here, DDL, the reaction product between Fluoral-P and formaldehyde, exhibits fluorescence from 450 to 650 nm with a maximum intensity at a wavelength of 510 nm.[6] According to the slow photon effect, if any fluorescence wavelength in the range from 450 to 650 nm matches the band edge of the photonic bandgap of the PC, the intensity at the fluorescence wavelength will be greatly enhanced.[6,10,17] The wavelength at the band edge of 50 nm-350IOPC cannot be read directly from Fig. 10; however, the reflectance at 463 nm greatly increased. These results suggest that 463 nm is the band edge of the photonic bandgap of 50 nm-350IOPC. Furthermore, the fluorescence at 510 nm, at which the maximum fluorescence intensity of DDL is observed, is the most effective for obtaining a lower detection limit and increasing the response speed.

Figure 17 shows the reflection spectrum of 500IOPC. The peak wavelength was 695 nm and a blue band edge was observed at around 650 nm.

Figures 18 and 19 show the reflection spectra of 350IOPC and 500IOPC with infiltrated Fluoral-P before and after formaldehyde exposure, respectively. In Fig. 18, the reflectance at around 480 nm increases. In Fig. 19, the reflectance at around 765 nm increases, whereas

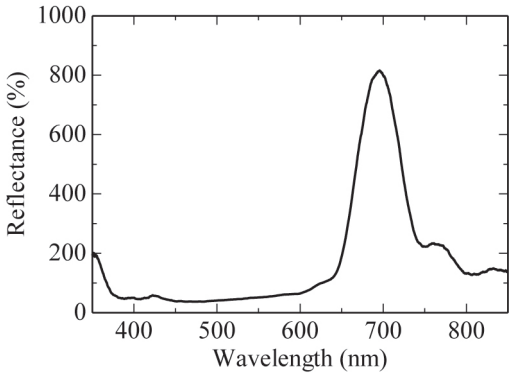

Fig. 17. Reflection spectrum of 500IOPC.

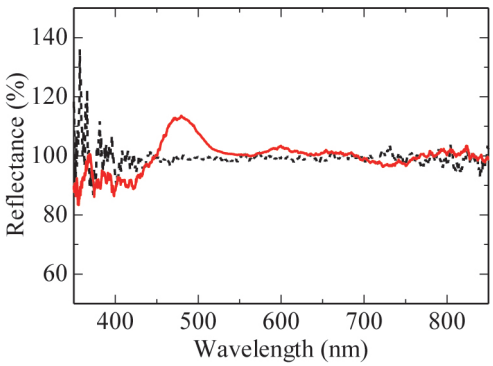

Fig. 18. (Color online) Reflection spectral change on 350IOPC before (dashed black line) and after (red line) formaldehyde exposure.

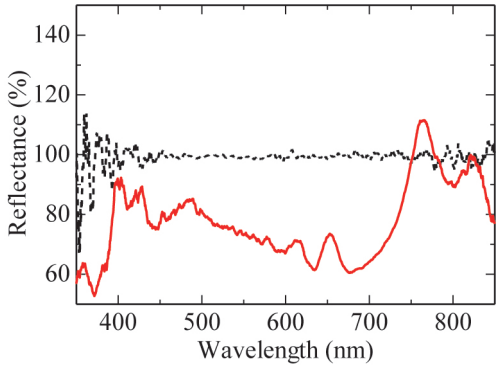

Fig. 19. (Color online) Reflection spectral change on 500IOPC before (dashed black line) and after (red line) formaldehyde exposure.

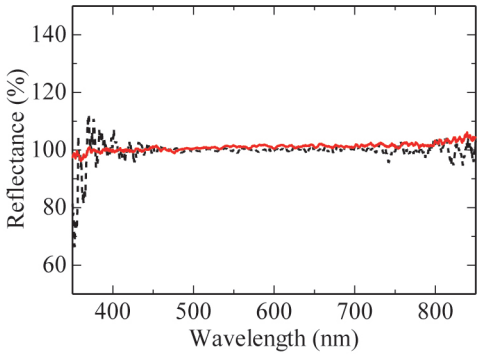

Fig. 20. (Color online) Reflection spectral change on glass slide before (dashed black line) and after (red line) formaldehyde exposure.

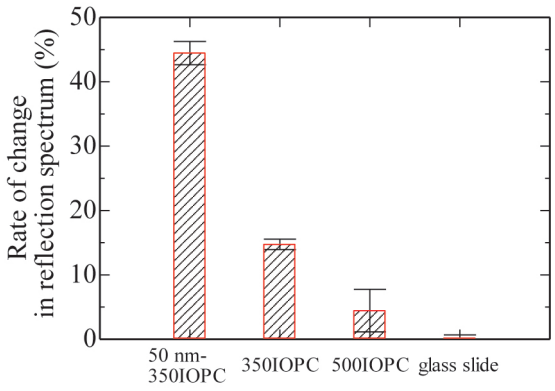

Fig. 21. (Color online) Rates of spectral changes on 50 nm-350IOPC, 350IOPC, 500IOPC, and glass slide.

it decreases at other wavelengths; it is possible that light energy was consumed to excite DDL. Figure 20 shows the reflection spectra of the glass slide modified with Fluoral-P before and after formaldehyde exposure. The reflection spectrum did not change upon exposure to formaldehyde because Fluoral-P does not react with gaseous formaldehyde.

Figure 21 shows the relative reflection spectral changes on 50 nm-350IOPC, 350IOPC, 500IOPC, and the glass slide upon exposure to formaldehyde. The relative reflection spectral change on 50 nm-350IOPC was obtained using the reflectance at 463 nm, whereas the reflectances at 480 and 765 nm were used for 350IOPC and 500IOPC, respectively. A significant change in reflectance on the glass slide was not observed at any wavelength; therefore, the value at 510 nm, which gives the maximum fluorescence intensity of DDL, was chosen. From Fig. 21, the rates of reflection spectral changes on 50 nm-350IOPC and 350IOPC were higher than that on 500IOPC. Therefore, detection using a fluorescent substance should involve the slow photon effect, and it is important to fabricate IOPCs while considering that the edge on the photonic bandgap of the PC should be matched. Furthermore, the rate of reflection spectral change on 50 nm-350IOPC was much higher than that on 350IOPC. In addition to the enhancement of the reaction of the Fluoral-P-infiltrated IOPC with formaldehyde in the liquid phase by capillary condensation, the amount of Fluoral-P per unit volume and the porosity increased when mesopores were introduced into the IOPC. Therefore, introducing mesopores into IOPCs is advantageous.

4. Conclusions

In this study, IOPCs with mesopores were fabricated with the optimization of the size ratio of large to small PS nanoparticles used as the template of each IOPC and the concentration of the precursor forming the structure of the IOPC. The generation of cracks and defects on the obtained IOPCs was inhibited by using a co-assembly method. Fluoral-P was infiltrated into the IOPCs, and the edge of the photonic band gap on a 50 nm-350IOPC was matched with part

of the fluorescence wavelength range of DDL, which is a fluorescent compound resulting from the reaction between Fluoral-P and formaldehyde. It was found that introducing mesopores into 350IOPC with infiltrated Fluoral-P was effective for enhancing the signal in formaldehyde detection.

Acknowledgments

The observation of the IOPC film was observed using an SU8000 SEM system at the Center of Advanced Instrumental Analysis, Kyushu University.

References

1 H. Xu, P. Wu, C. Zhu, A. Elbaz, and Z. Z. Gu: J. Mater. Chem. C **1** (2013) 6087. https://doi.org/10.1039/c3tc30722k
2 C. Fenzl, T. Hirsch, and O. S. Wolfbeis: Angew. Chem. Int. Ed. **53** (2014) 3318. https://doi.org/10.1002/anie.201307828
3 I. A. Levitsky: Sensors **15** (2015) 19968. https://doi.org/10.3390/s150819968
4 T. Endo, Y. Yanagida, and T. Hatsuzawa: Sens. Actuators, B **125** (2007) 589. https://doi.org/10.1016/j.snb.2007.03.003
5 B. Hatton, L. Mishchenko, S. Davis, K. H. Sandhage, and J. Aizenberg: Proc. Natl. Acad. Sci. U.S.A. **107** (2010) 10354. https://doi.org/10.1073/pnas.1000954107
6 Y. Zhang, L. Mu, R. Zhou, P. Li, J. Liu, L. Gao, L. Heng, and L. Jiang: J. Mater. Chem. C **4** (2016) 9841. https://doi.org/10.1039/c6tc03862j
7 Y. Zhang, J. Qiu, R. Hu, P. Li, L. Gao, L. Heng, B. Z. Tang, and L. Jiang: Phys. Chem. Chem. Phys. **17** (2015) 9651. https://doi.org/10.1039/c4cp06019a
8 Z. Xie, K. Cao, Y. Zhao, L. Bai, H. Gu, H. Xu, and Z. Z. Gu: Adv. Mater. **26** (2014) 2413. https://doi.org/10.1002/adma.201304775
9 J. Wang, Q. Li, W. Knoll, and U. Jonas: J. Am. Chem. Soc. **128** (2006) 15606. https://doi.org/10.1021/ja067221a
10 W. K. Kuo, H. P. Weng, J. J. Hsu, and H. H. Yu: Appl. Sci. **6** (2016). https://doi.org/10.3390/app6030067
11 G. Mayonado, S. Mian, V. Robbiano, and F. Cacialli: 2015 Conf. Laboratory Instruction Beyond the First Year of College (2015) 60. https://doi.org/http://dx.doi.org/10.1119/bfy.2015.pr.015
12 F. Casanova, C. E. Chiang, C. P. Li, I. V. Roshchin, A. M. Ruminski, M. J. Sailor, and I. K. Schuller: Nanotechnology **19** (2008). https://doi.org/10.1088/0957-4484/19/31/315709
13 J. Wang, S. Ahl, Q. Li, M. Kreiter, T. Neumann, K. Burkert, W. Knoll, and U. Jonas: J. Mater. Chem. **18** (2008) 981. https://doi.org/10.1039/b715329e
14 L. Wang, Y. Wan, Y. Li, Z. Cai, H. L. Li, X. S. Zhao, and Q. Li: Langmuir **25** (2009) 6753. https://doi.org/10.1021/la9002737
15 S. J. Yeo, G. H. Choi, and P. J. Yoo: J. Mater. Chem. A **5** (2017) 17111. https://doi.org/10.1039/C7TA05033J
16 B. J. Compton and W. C. Purdy: Anal. Chim. Acta **119** (1980) 349. https://doi.org/10.1016/S0003-2670(01)93636-0
17 R.-Q. Xing, L. Xu, Y.-Q. Zhu, J. Song, W.-F. Qin, Q.-L. Dai, D.-L. Liu, and H.-W. Song: Sens. Actuators, B **188** (2013) 235. https://doi.org/10.1016/j.snb.2013.07.024

About the Authors

Yuto Komori received his B.E. and M.E. in electrical engineering from Kyushu University, Japan, in 2016 and 2018, respectively. He now works for Murata Manufacturing.

Hiroaki Murakami received his B.E. in electrical engineering from Kyushu University, Japan, in 2017. He is now developing an inverse opal PC for ammonia gas detection.

Taiki Kimura received his B.E. in electrical engineering from Kyushu University, Japan, in 2017. He is now studying the application of polymer-based PCs.

Takeshi Onodera received his B.A. degree from Toyama University of International Studies, Toyama, Japan, in 1996. He received his M.Ed. degree in technology education and Ph.D. degree in engineering from Kanazawa University in 1998 and 2001, respectively. He is now an associate professor at Kyushu University. He is a member of the Institute of Electrical Engineers of Japan, the Electrochemical Society of Japan, the Japan Explosives Society, and the Japan Society of Applied Physics. (onodera@ed.kyushu-u.ac.jp)